Shear deformation and plasticity of metallic glass under multiaxial loading

F.F. Wu [a], Z.F. Zhang [a,*], J. Shen [b], S.X. Mao [a,c]

[a] *Shenyang National Laboratory for Materials Science, Institute of Metal Research, Chinese Academy of Sciences, 72 Wenhua Road, Shenyang 110016, China*
[b] *School of Materials Science and Engineering, Harbin Institute of Technology, Harbin 150001, China*
[c] *Department of Mechanical Engineering, University of Pittsburgh, 648 Benedum Hall, Pittsburgh, PA 15261, USA*

Abstract

The evolution of multiple shear bands in a Zr-based metallic glass under multiaxial loading was systematically investigated by the small punch test. Unlike the fast propagation of the individual shear band and catastrophic failure of the metallic glass under uniaxial tensile or compressive loading, the metallic glass can be controlled to create regularly arrayed fine multiple shear bands under multiaxial loading. The distribution of the shear bands displayed a cobweb-like pattern along radial and circumferential directions. A large equivalent plastic strain (19.6%) was achieved in the metallic glass under multiaxial loading, which was far higher than that gained under uniaxial compressive loading. The multiaxial loading method was also applied to evaluate the mechanical properties of the annealed Zr-based metallic glass. Three types of failure modes were observed in the as-cast or annealed specimens: circumferential and radial shear failure, and radial normal (cleavage) failure. In contrast with uniaxial tension and compression, the multiaxial loading by small punch test was found to be very suitable for the evaluation of the mechanical properties of metallic glasses and, further, to distinguish the transition from ductility to brittleness more accurately.

1. Introduction

Metallic glasses have evoked extensive research interest because of their particular physical and chemical properties [1–5]. Under uniaxial tension, the metallic glass fails catastrophically by the fast propagation of an individual shear band with a fracture angle larger than 45°, exhibiting near zero macroscopic plasticity, though the shear band itself has high microscopic plasticity. Under uniaxial compression, there are also few shear bands, and the specimen quickly fails by the propagation of an individual shear band with a fracture angle smaller than 45°, displaying limited plasticity (about 2%) [6,7]. When the aspect ratio of the

compressive specimen is smaller than 1, due to the constraint of the upper and lower tungsten carbide plates, profuse shear bands are formed. Therefore the metallic glass can exhibit a remarkably larger plastic strain than that with an aspect ratio of 2 under uniaxial compression [8–13]. Bending is considered as an inherently stable deformation method, as the stress to drive shear bands diminishes as the shear band approaches the neutral axis [14,15]. Bend ductility can be achieved only if the specimen's dimension is below a critical value, suggesting a strong size effect on the bend ductility [16,17]. Indentation, especially instrumented nanoindentation, has been extensively used to study the evolution of shear bands and the plastic-deformation instability, i.e. serrated flow, in metallic glasses [18–20]. It was found that profuse and regular shear bands formed in the region beneath the indenter [21,22], which is

---
* Corresponding author. Tel: +86 24 23971043; fax: +86 24 23891320.
  E-mail address: zhfzhang@imr.ac.cn (Z.F. Zhang).

fundamental to understanding the shear band morphology and is useful in the investigation of plastic-deformation behavior of metallic glasses. In contrast to the catastrophic shear failure under uniaxial compression, metallic glass produced more shear bands with large inelastic deformation of more than 10% with confined compression, demonstrating the ductile nature of metallic glass under constrained conditions [23].

Recently, the mechanical properties of metallic glass under biaxial tensile loading was studied by the small punch technique [24]. It was found that metallic glass can be controlled to create regularly arrayed fine multiple shear bands using this test, indicating that metallic glass essentially has a good plastic-deformation ability and thus high ductility under suitable loading conditions. The findings showed that the initiation and propagation of shear bands in metallic glass strongly depend on the stress state. In the present work, a systematic investigation is conducted to study the evolution of multiple shear bands of a Zr-based metallic glass under multiaxial loading by the small punch test, and the mechanical properties of the metallic glasses annealed at different temperatures are further evaluated for better understanding of the ductile-to-brittle transition of metallic glass.

2. Experimental

The Zr-based metallic glass alloy with a nominal chemical composition of $Zr_{52.5}Ni_{14.6}Al_{10}Cu_{17.9}Ti_5$ was prepared by arc-melting. The final ingots have a rectangular shape, with dimensions of $60 \times 30 \times 3$ mm^3. The as-cast specimens were sealed in vacuum quartz tubes and annealed at 623, 653 or 693 K for 1 h. The quartz tubes were then removed from the furnace and cooled in air down to room temperature. A Perkin Elmer DSC-7 differential scanning calorimeter (DSC) was used to determine the glass transition and the crystallization behavior of the as-cast metallic glass ingot. DSC data (not shown here) indicate that the glass transition and the first crystallization temperatures are 641 and 699 K, respectively. The microstructure of the as-cast and annealed specimens was characterized by using a Leo Supra 35 scanning electron microscope (SEM), as well as a Rigaku X-ray diffractometer (XRD) with Cu K_α radiation. XRD patterns showed that the as-cast alloy had a fully glassy structure, as shown in Fig. 1. The specimens annealed at 623 and 653 K had fully glassy structures too, but the one annealed at 693 K exhibited obvious crystallization features. Mechanical properties of the as-cast and annealed specimens were characterized using the small punch testing technique, as illustrated in Fig. 2. The metallic glass specimen disk was clipped in the upper (3.0 mm in diameter) and lower (5.0 mm in diameter) dies. The steel ball was 3.0 mm in diameter. Specimens 0.7 mm in thickness and 10 mm in diameter were cut from the metallic glass ingot by an electric spark cutting machine, then were ground and polished to be 0.3–0.5 mm thick by 2.5 μm abrasive paste. The small punch tests were performed with
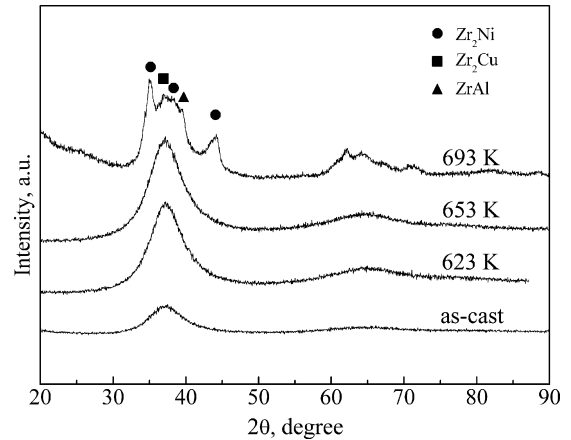

Fig. 1. XRD patterns taken from the as-cast specimen and the specimens annealed at 623, 653 and 693 K, respectively.
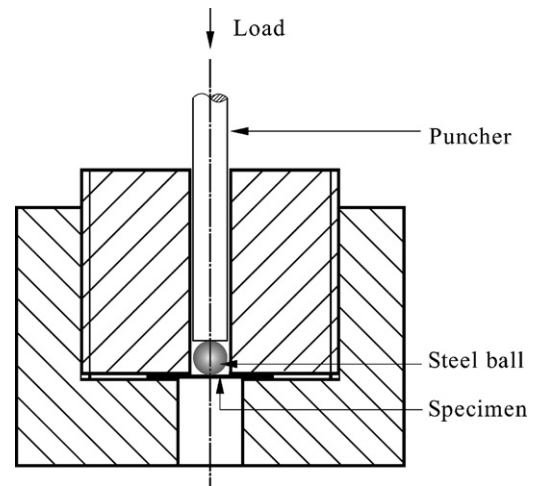

Fig. 2. Illustration of the small punch test: the metallic glass specimen disk was clipped in the upper and lower dies.

an MTS810 testing machine at room temperature. All the tests were conducted using a constant crosshead rate of about 0.001 mm s^{-1}. After the punch tests, all the specimens were observed by SEM and an Olympus LEXT OLS3000 laser confocal scanning microscope (LCSM) to reveal the deformation and fracture features and quantitatively measure the height of the shear offset.

3. Results

3.1. Evolution of shear bands under the small punch test

Fig. 3 shows the load–deflection (F–f) curves of the as-cast Zr-based metallic glass specimens subjected to the small punch test. The curve can be generally divided into two regions: an elastic region and a plastic region [25], marked A and B in Fig. 3. In the elastic region, the initial stiffness, k, is about 1.65 kN mm^{-1} on average, which is determined by the elastic modulus, E, the thickness t of the specimen and the geometry of the dies. Based on the
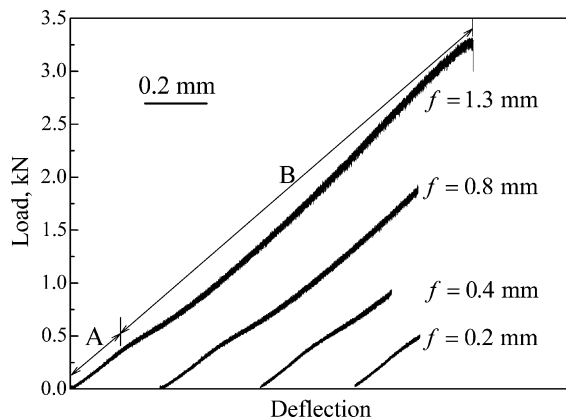
Fig. 3. Load–deflection curves achieved by the small punch test for the as-cast specimen with different deflections: 1.3, 0.8, 0.4 and 0.2 mm. The regions marked A and B represent the elastic and plastic regions.

bending theory of thin plate [26], the initial stiffness k can be expressed as

$$k = \frac{4\pi t^3 E}{3\lambda a^2 (1 - \mu^2)} \tag{1}$$

where a, μ and λ are the radius of the lower die, the Poisson ratio of the specimen and the non-dimensional coefficient of correction. In the plastic region, by comparing the load–deflection curve with the plastic bending model and the plastic membrane stretching model based on the perfect

rigid plastic model of Onat and Haythornthwaite [27], the experimental results are initially in agreement with those of the plastic bending and then fall between the plastic bending and the membrane stretching solution. When the load reaches the peak value, the specimens lose their load-carrying capacity immediately and fall abruptly into failure.

Fig. 4 shows the SEM images of the lower surfaces of the small punch specimens with different deflections. It can be seen that the radial shear bands appear first with a small deflection (see Fig. 4a and b), and then circumferential shear bands start to form with increasing deflection (see Fig. 4c and d). Fig. 5 shows three typical SEM images on the lower surface of the specimen with a deflection of $f = 0.8$ mm. In the central region (marked with A in Fig. 4c), the shear bands are multiple and disordered, as shown in Fig. 5a. With increasing distance away from the center, as indicated by region B of Fig. 4c, the shear bands are very dense and regular in both the radial and circumferential directions, forming a cross-weave structure, as shown in Fig. 5b. In region C of Fig. 4c, the circumferential shear bands disappear and only radial shear bands can be seen. Meanwhile, the shear deformation of the radial shear bands gradually became weak and disappeared, as shown in Figs. 4 and 5c.

By analyzing the evolution and morphology of the shear bands on specimens with different deflections, it is found that the region of shear bands spreads rapidly at first and
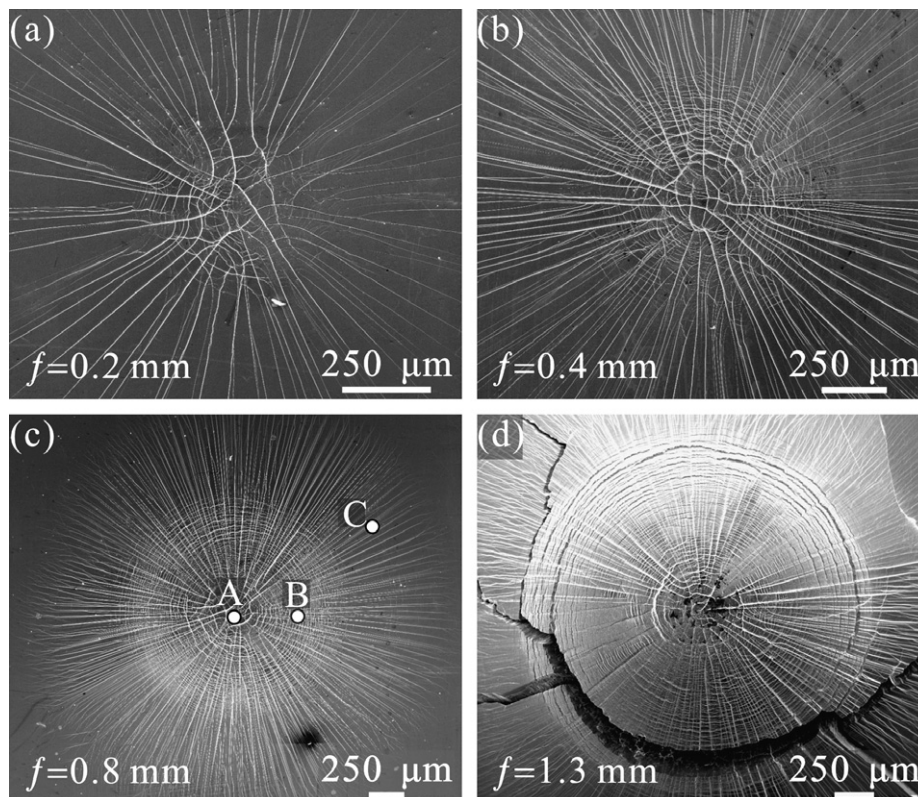

Fig. 4. Morphology of shear bands on the lower surface for the metallic glass specimens with deflections: of (a) 0.2 mm, (b) 0.4 mm, (c) 0.8 mm and (d) 1.3 mm.
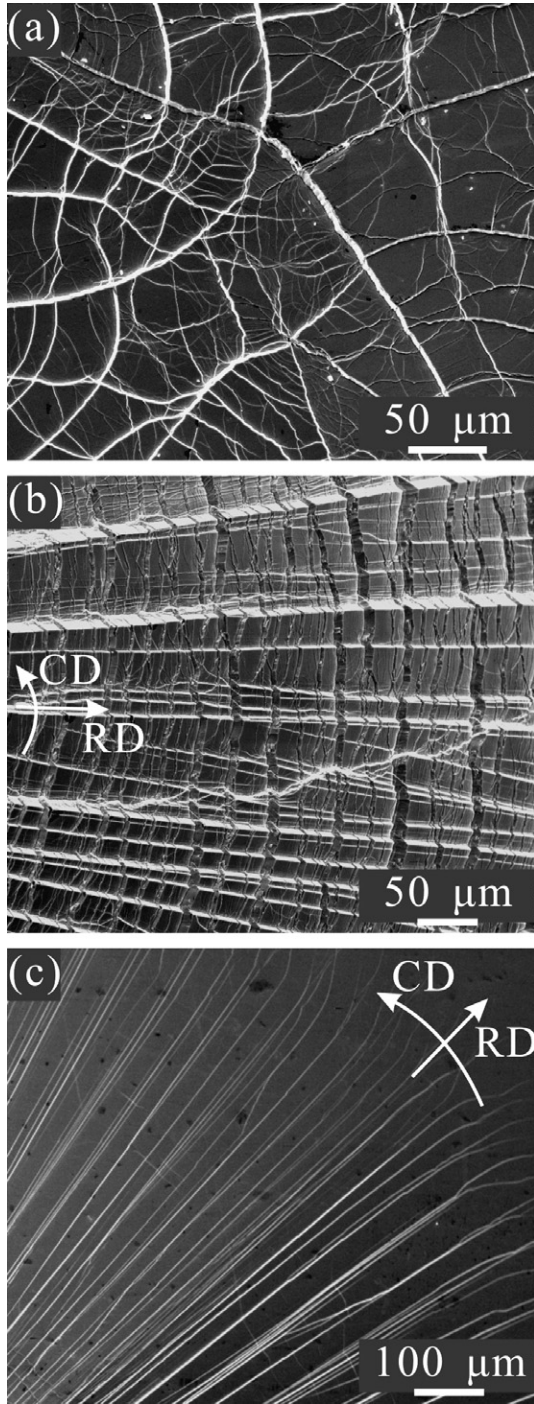
Fig. 5. High-magnification SEM images of the three typical regions in the as-cast specimen with 0.8 mm deflection: (a) in region A of Fig. 4, the shear bands are disordered; (b) in region B of Fig. 4, dense, regular radial and circumferential shear bands coexist; and (c) in region C of Fig. 4, circumferential shear bands vanish and only radial shear bands can be seen. Here CD and RD denote the circumferential and radial directions respectively.

then increases slowly with further deflecting, as shown in Fig. 6a. The width D_R of the region of radial shear bands is over three times as large as the width D_C of the region of the circumferential shear band in the case of $f = 0.2$ mm, then the ratio $R = D_R/D_C$ of D_R–D_C

decreases to 1.8 when the deflection rises to 1.3 mm, as shown in Fig. 6b. The density of radial shear bands (ρ) can be expressed as

$$\rho = \frac{N}{2\pi} \qquad (2)$$

where N is the total number of the radial shear bands. With the deflection increasing, the density of the radial shear bands initially increased almost linearly, but finally reached a saturation density of about 83.4 rad^{-1} at $f = 0.8$ mm. With further deformation, the density of radial shear bands was maintained nearly constant even when the specimen failed at a deflection $f = 1.3$ mm. Analysis based on the observations under SEM and LCSM indicated that the maximum shear offset increased monotonically with the deflection, as shown in Fig. 6d. The radial and circumferential shear offsets reached up to 17.3 and 26.6 μm, respectively, at the failure deflection of $f = 1.3$ mm. Assuming that the average thickness of the shear band was about 10–100 nm [28–32], the shear plastic strain within an individual shear band was estimated to be about 10^4–10^5%, which is far higher than that 10^2–10^3% reported by Chen et al. [33].

By calculating the thickness reduction of the deformed specimen, the equivalent plastic strain ε_q was obtained and can be expressed as follows:

$$\varepsilon_q = \ln(t_0/t') \qquad (3)$$

Here t_0 and t' are the thicknesses of the specimen before and after deformation [25]. Fig. 7 shows the equivalent plastic strain of the specimen at different deflections. It is interesting to note that the maximum ε_q did not occur in the center of the specimens. For example, at a deflection $f = 0.2$ mm, the maximum ε_q was near 1.1%, occurring at a location about 0.3 mm away from the center of the specimen. With increasing deflection, the positions with the maximum ε_q shifted outwards from the center of the specimen.

3.2. The effect of annealing on the shear bands of metallic glass

After the small punch tests above, some specimens were annealed to show the effect of annealing on the evolution of the shear bands. Fig. 8a shows load–deflection curves of the as-cast and annealed Zr-based metallic glasses. It can be seen that the load and deflection to failure obviously decrease with increasing annealing temperature. The curves for the specimens annealed at 623 and 653 K still exhibited a long plastic region; however, the specimen annealed at 693 K failed in the elastic region without any obvious plastic-deformation. To compare the deformation energy absorbed during the small punch test, the work to failure, W, was calculated by
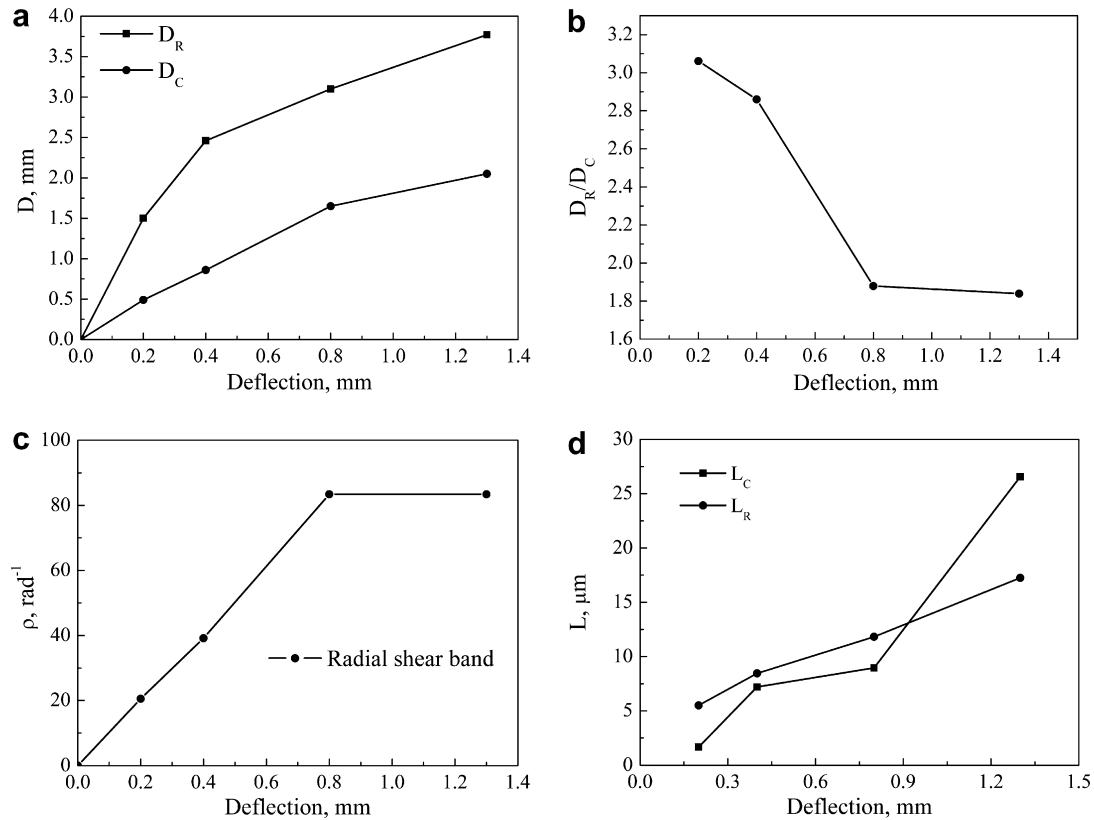
$$W = \int F\,df \qquad (4)$$

Fig. 6. Quantitative analysis on the shear bands of the as-cast specimens with different deflections: (a) the dependence of shear bands width (D) on the deflection; (b) the ratio of radial shear bands width (D_R) to the circumferential shear bands width (D_C) on the deflection; (c) the radial shear bands density (ρ) on the deflection; and (d) the radial and circumferential shear offset (L_R and L_C) on the deflection.
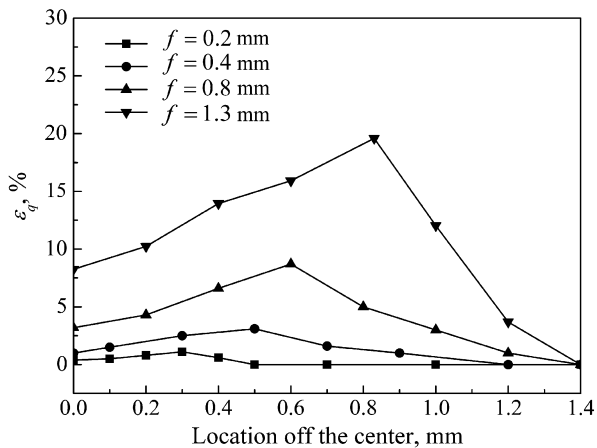

Fig. 7. Dependence of equivalent plastic strain (ε_q) on the location from the center of the specimens.

where F and f denote the load and the deflection to failure. Fig. 8b is the work to failure of the as-cast and annealed Zr-based metallic glasses. The work to failure values are 2.42, 1.91, 1.05 and 0.02 J for the as-cast glass and the specimens annealed at 623, 653 and 693 K, respectively, showing an obvious decreasing tendency as the annealing temperature increased. The work to failure for the specimen annealed at 693 K is almost zero, indi-

cating that the load capacity of the annealed specimen became very small.

Fig. 9 shows the SEM images of the deformation patterns on the lower surfaces of the as-cast and annealed specimens. It can be seen that the as-cast and metallic glasses annealed at 623 K failed in a similar mode: a primary circumferential crack and several secondary radial cracks. Finally, the densities of the radial and circumferential shear bands became very high. High-resolution SEM showed that there was a wide stable shear region (A in Fig. 10a and b) in the circumferential crack, followed by a tensile fracture region with radiating vein-like patterns (B in Fig. 10a and b). The width of the stable shear region can be as high as ~70 μm for the as-cast and some annealed specimens, which is far higher than 22 μm gained under uniaxial tension [34]. When the annealing temperature increased to 653 K, the specimen always failed by shearing only along the radial directions, and there was no visible circumferential crack. The radial crack was also characterized by a stable shear region with a width of about 25 μm and a tensile radiating vein-like pattern following the stable shear region, marked A and B, respectively, in Fig. 10c. When the annealing temperature was increased up to 693 K, the specimen failed along a few radial cracks without any visible radial and circumferential shear bands, and the cracks were perpendicular to the sur-
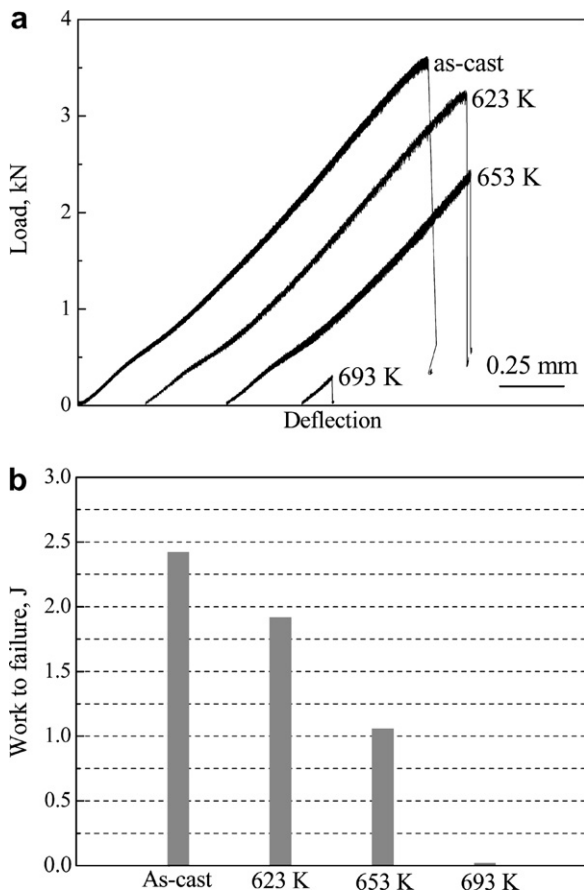
Fig. 8. Effect of annealing on the mechanical properties under the small punch test: (a) load–deflection curves achieved by the small punch test for the as-cast specimen and the specimens annealed at 623, 653 and 693 K; and (b) work to failure calculated from the load–deflection curves for the as-cast specimen and the specimens annealed at 623, 653 and 693 K.

By measuring the thickness reduction, the equivalent plastic strain was achieved for the as-cast and annealed specimens, as shown in Fig. 12 and Table 1. The equivalent plastic strain decreased with increasing annealing temperature. The maximum equivalent plastic strain to failure is 19.6%, 20.4%, 12.5% and 0% for the as-cast specimen and the specimens annealed at 623, 653 and 693 K, respectively. The locations with the maximum equivalent plastic strain are 0.82, 0.75 and 0.63 mm away from the center of the specimens for the as-cast specimen and the specimens annealed at 623 and 653 K, respectively, indicating a gradual transition of maximum equivalent plastic strain from the outside to the center of the specimens with increasing annealing temperature.

4. Discussion

From the experimental observations above, it is obvious that there exist profuse multiple shear bands with regular morphology after small punch testing. The creation of multiple shear bands should result from the complex biaxial tensile stress state applying to the metallic glass specimens [24]. As shown in Fig. 13, the lower surface of the small punch specimen is in a biaxial tensile stress state, including radial normal tensile stress σ_r and circumferential normal tensile stress σ_θ. Both σ_r and σ_θ can be resolved into a shear stress and a normal stress on any stress plane; and the maximum shear stress occurs on the plane with a certain angle to the punch direction. When the maximum shear stress rises to the critical shear strength of the metallic glass with increasing loading, shear bands will first initiate and then propagate along the radial direction if considering the Tresca criterion. Similarly, the radial normal stress σ_r can also be resolved into a normal stress and a maximum shear stress. When the maximum shear stress increases to the critical shear strength of the metallic glass, circumferential shear bands will be created as circles around the center of the punched area. However, it is found that the shear angle is slightly larger than 45°, which implies that the Tresca criterion is unsuitable for the shear deformation of metallic glass. It is suggested that the pressure-dependent yield criterion, i.e. the Mohr–Coulomb criterion, could explain the deviation of the shear angle from the maximum shear stress direction [6,7,29,38,39]. Due to the circumferential constraint of the clips, the radial shear bands cannot propagate forward to the rim of the specimen, leading to the formation of denser radial shear bands. Meanwhile, multiple circumferential shear bands can be created due to the constraint imposed by the steel ball under the upper surface of the small punch specimen; therefore, the interactions of both radial and circumferential shear bands along the two directions further propagate individual shear bands, resulting in the well-developed shear bands that can been seen from the long shear offset in Figs. 5 and 10.

It is well known that crystalline metallic materials can exhibit great macroscopic plastic deformation due to multiple and cross slip. However, metallic glass can also create

face plane of the specimen. This indicates that the specimen became extremely brittle when it was crystallized at high temperature, which was often observed in the annealed metallic glasses [35]. High-resolution SEM images of the cracks exhibited typical brittle fracture features, forming an initial rough region, followed by a mirror region and an unstable propagation region [36]. The evolution of radial and circumferential shear bands and the failure of the as-cast and annealed Zr-based metallic glass seen here are very similar to that observed in indentation studies by Jana et al. [37], suggesting a transition in the nature of the deformation mechanism due to annealing.

With increasing annealing temperature up to 623 and 653 K, the width of the shear bands reduced slightly, as shown in Fig. 11 a. However, from Fig. 11b it can be seen that the shear offset changed: the circumferential shear offset is longer than the radial one for the as-cast specimen or the specimen annealed at 623 K, which corresponds with the primary circumferential failure, as indicated in Figs. 9a and b 10a and b; but for the specimen annealed at 653 K, the radial shear offset is far wider than the circumferential one, which is consistent with the radial shear failure of the specimen, as shown in Figs. 9c and 10c.
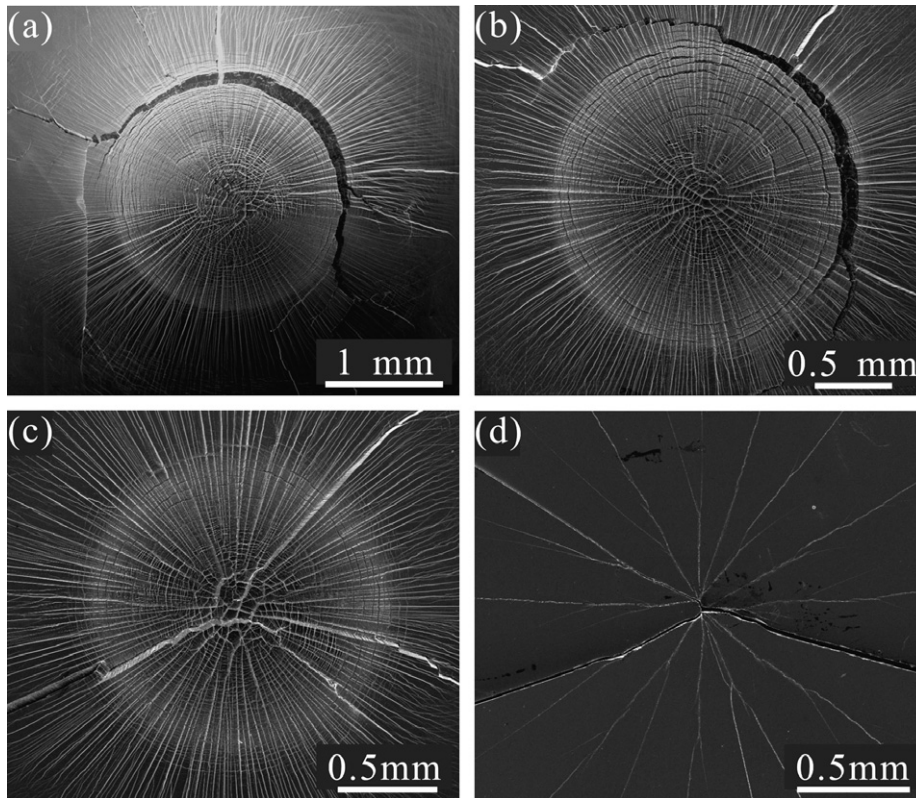
Fig. 9. SEM images of the lower surface for (a) the as-cast specimen and the specimens annealed at (b) 623 K, (c) 653 K and (d) 693 K.
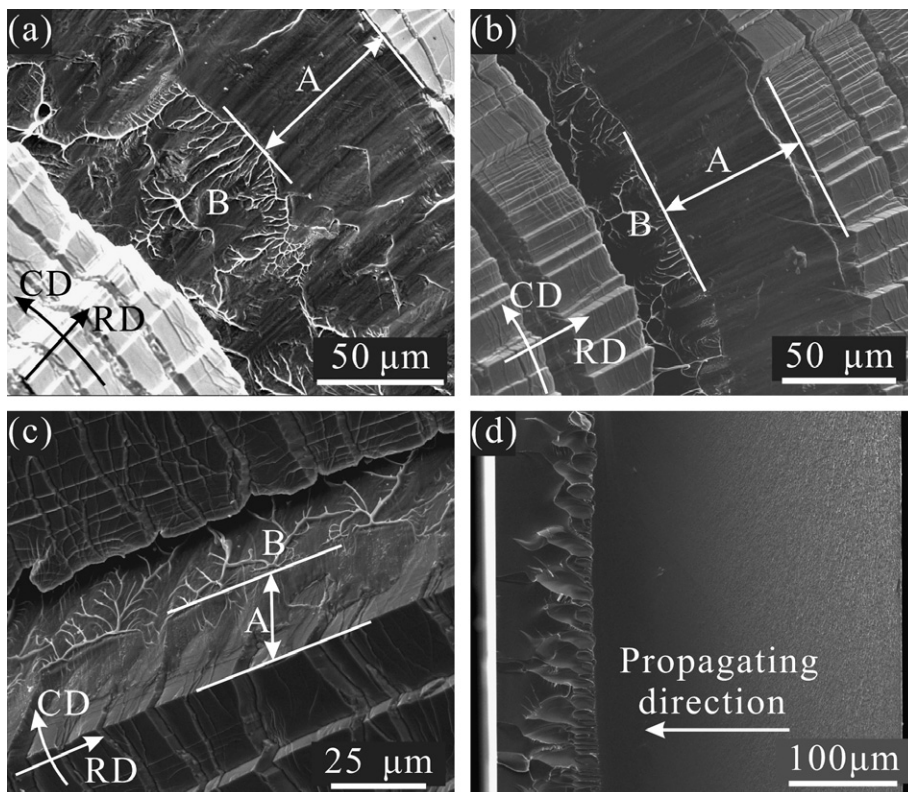

Fig. 10. High-magnification SEM images of the cracks for the as-cast specimen and the specimens annealed at (b) 623 K and (c) 653 K, and (d) cross-sectional SEM image for the specimen annealed at 693 K.
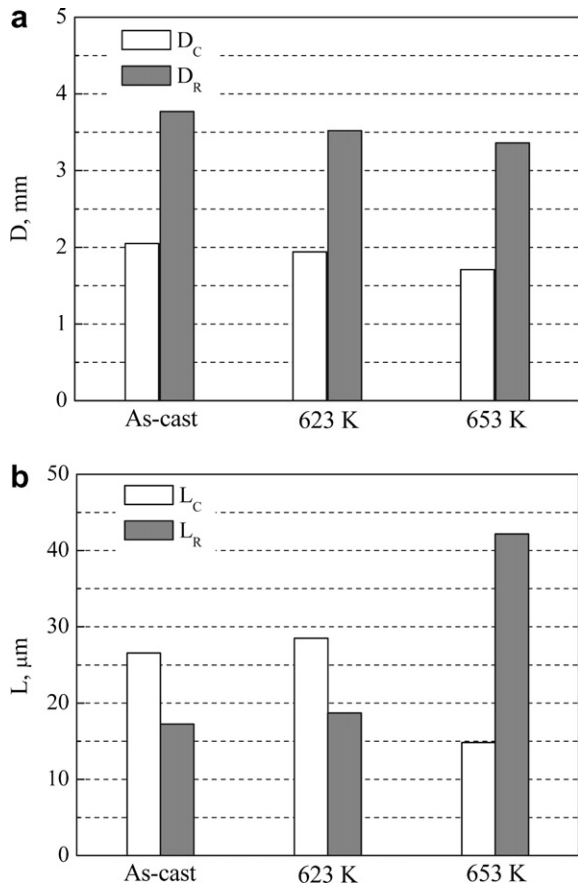
Fig. 11. Effect of annealing temperature on the morphology of the shear bands: (a) radial and circumferential shear bands width; and (b) shear offset for the as-cast specimen and the specimens annealed at 623 and 653 K.
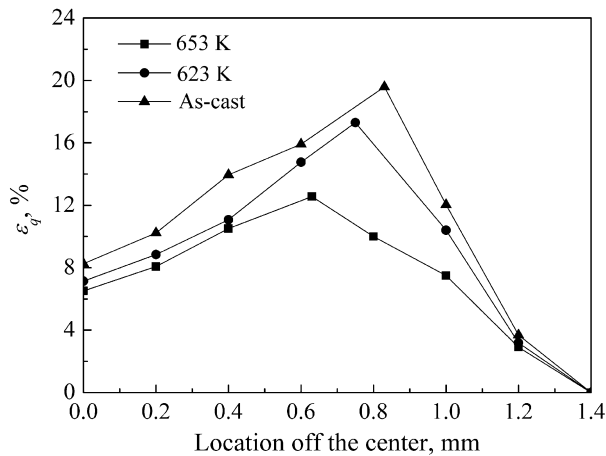

Fig. 12. Dependence of equivalent plastic strain on the location from the center for the as-cast specimen and the specimens annealed at 623, 653 and 693 K.

dense multiple regular shear bands under biaxial tension, and exhibit large plastic-deformation capability, which is functionally similar to the multiple slip in crystalline metallic materials. Recently, Guo et al. [40] found that metallic glass can deform uniformly to a high strain level up to

15%, as seen either by shear deformation or by an obvious necking feature under tension when the sample gauge decreased to a small dimension of about $100 \times 100 \times 250 \text{ nm}^3$, indicating a size-dependence of the deformation mechanism in metallic glass materials. Interestingly, the necking phenomenon was also observed in the metallic glass under biaxial tension, and is a typical feature found only in ductile metallic materials, as shown in Fig. 14. The equivalent fracture plastic strain ε_{qf} was obtained by measuring the thickness change at the fracture point (necking region) in the specimen. For the present metallic glass specimen and the small punch test sets, the equivalent fracture plastic strain can be empirically expressed as [25]

$$\varepsilon_{qf} = 0.028 \times (f/t_0)^{1.5} \tag{5}$$

where f and t_0 are the central deflection and the thickness of the specimen before deformation. From Eq. (5) it is obvious that, given a certain specimen thickness, the equivalent fracture plastic strain increases exponentially with the central deflection of the specimens. Further investigation confirms that the empirical equation above is also suitable to estimate the maximum equivalent plastic strain of the small punch specimen at an arbitrary deflection.

On the other hand, most metallic glass specimens exhibited two failure modes at room temperature: shear fracture and normal fracture under uniaxial tension, or shear fracture and split fracture (distensile fracture) under uniaxial compression [41–44]. However, the current work showed that there are three failure modes under biaxial tension loading for the as-cast and annealed Zr-based metallic glass: circumferential and radial shear fracture, and radial normal fracture, as shown in Fig. 9. The specimens that failed in the circumferential shear mode, such as the as-cast specimen and that annealed at 623 K, have the highest density of shear bands in both the radial and circumferential directions. For the specimens that failed in the radial shear mode, such as the specimen annealed 653 K, though there are still profuse radial and circumferential shear bands, the density of shear bands is relatively lower than that in the specimen failed in the circumferential shear mode. For the specimen that failed in the normal fracture, such as the specimen annealed at 693 K, there is no shear band in a radial or circumferential direction. Under uniaxial tension or compression, the as-cast specimen and those annealed at 623 and 653 K often failed in the same mode: shear fracture [44]. However, under biaxial tension, the as-cast specimen and that annealed at 623 K failed in the circumferential shear mode, while the specimen annealed at 653 K only failed in the radial shear mode. This implies that biaxial tension loading can effectively distinguish the mechanical properties and failure mechanisms of the metallic glass specimens more accurately. The effect of annealing on the mechanical properties of the small punch specimen is similar to its effect on the uniaxial tensile properties of the annealed dendrite-reinforced Zr-based metallic glass composite [44].

Table 1
Mechanical properties of the as-cast and annealed Zr-based metallic glasses achieved by the small punch tests

Specimen n	Width of shear bands (mm)		Shear offset (µm)		$\varepsilon_{p,Max}$ (%)	Work to failure (J)
	Circumferential direction	Radial direction	Circumferential direction	Radial direction		
A	2.05	3.77	26.6	17.3	19.6	2.42
B	1.94	3.52	28.5	18.7	20.4	1.91
C	1.71	3	14.84	42.2	12.5	1.05
D	–	–	0	0	0	0.02

A: the as-cast specimen; B: the annealed specimen at 623 K; C: the annealed specimen at 653 K; and D: the annealed specimen at 693 K.
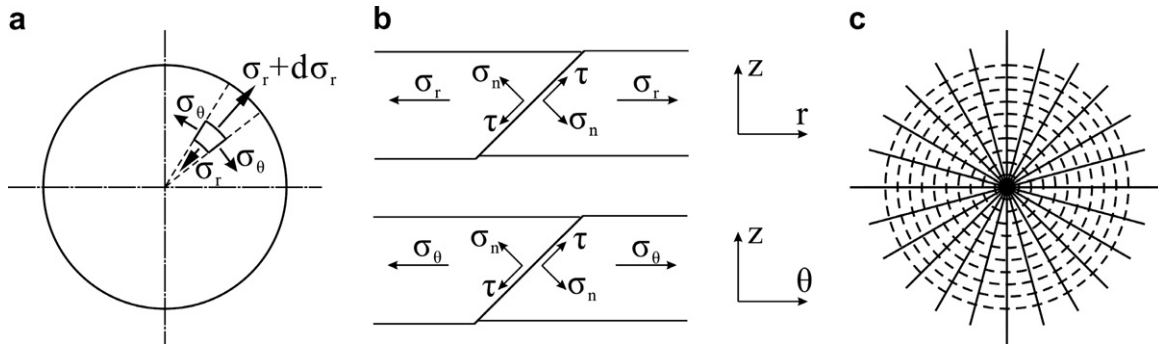

Fig. 13. Illustrations of (a) the stress state under small punch loading; (b) the resolution of the biaxial tensile stress; and (c) the shear bands morphology in the small punch specimens, where r, θ and z denote the radial, circumferential and the thickness directions of the specimens, respectively.
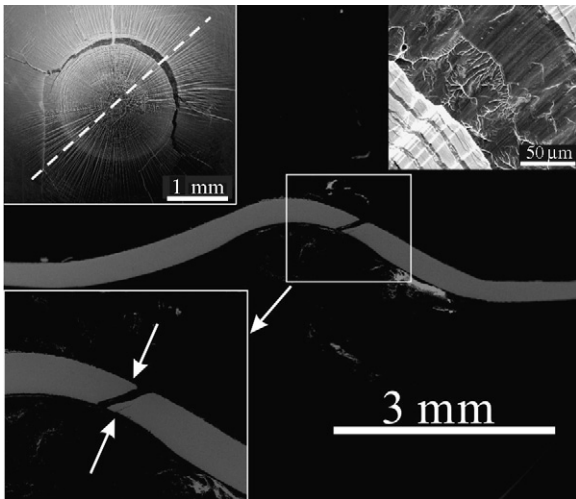

Fig. 14. SEM image of the cross section for the as-cast specimen.

To analyze the difference in the failure modes, a shear-cleavage coefficient, α, has been proposed [45],

$$\alpha = \tau_0/\sigma_0 \tag{6}$$

where τ_0 and σ_0 are the critical shear strength and the critical cleavage strength, respectively. It is an intrinsic mechanical constant of the material. Under tensile loading, the parameter $\alpha = \tau_0/\sigma_0$ is related to the tensile fracture angle, θ_T [45], as shown below:

$$\theta_T = \frac{\pi}{2} - \frac{1}{2}\arctan\left(\frac{\sqrt{1-2\alpha^2}}{\alpha^2}\right) \quad (0 < \alpha = \tau_0/\sigma_0 \leqslant \sqrt{2}/2)$$

$$\tag{7a}$$

$$\theta_T = 90° \quad (\alpha = \tau_0/\sigma_0 \geqslant \sqrt{2}/2) \tag{7b}$$

From Eq. (7), it is apparent that the tensile fracture angle θ_T strongly depends on the parameter α. In the case of a small α ($0 < \alpha = \tau_0/\sigma_0 < \sqrt{2}/2$), the metallic glass shears more easily and often fails in shear mode. Also, the smaller α is, the more easily shear deformation takes place, and the tensile fracture angle is between 45° and 90°, as illustrated in Fig. 15a. With increasing α, shear deformation becomes more and more difficult. In the case of a large α ($\alpha \geqslant \sqrt{2}/2$), the metallic glass should fail in normal fracture mode with a constant tensile fracture angle of 90° [44,45], as illustrated in Fig. 15b. As far as the present Zr-based metallic glass specimens are concerned, the critical cleavage strengths for the as-cast specimen and the specimens annealed at low temperature are still relatively high. Thus, the shear-cleavage coefficient α is still not large, leading to the easy occurrence of shear deformation in both radial and circumferential directions, as shown
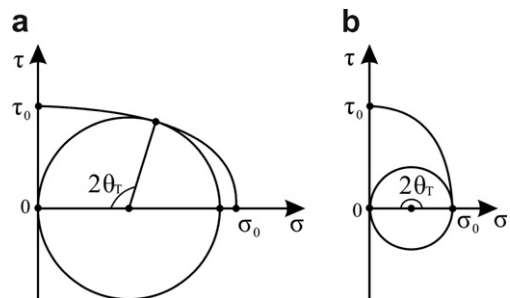

Fig. 15. Illustration of (a) shear failure condition and (b) normal (cleavage) failure condition.

in Figs. 9a and b and 10a and b. With increasing annealing temperature, due to structural relaxation, the free volume reduces [5,46], it is difficult to form and propagate a shear transformation zone under pressure, and the reduction in the free volume also decreases the mobility of the surrounding atoms, leading to a decrease in the critical cleavage strength σ_0 [44,45]. Therefore, the shear-cleavage coefficient α increases, resulting in shear deformation becoming relatively more difficult, which can be seen from the deformation of the 653 K annealed specimen, as shown in Figs. 9c and 10c. Circumferential deformation becomes difficult and the specimen fails only in the radial direction, which can also be seen from the shear offset for the specimen annealed at 653 K in Fig. 11. The density of shear bands decreases with increasing annealing temperature, which is similar to the considerable decrease in the density of the shear bands in the annealed $Zr_{41.2}Ti_{13.8}Cu_{12.5-}Ni_{10}Be_{22.5}$ alloy [47]. It was suggested that the ductile to brittle transition in annealed metallic glass should be attributed to the free volume reduction of the annealed glasses, and the minimum amount of free volume required for extensive plasticity (and hence high toughness) in metallic glasses is strongly dependent on temperature [5,48]. Moreover, for the specimen annealed above the crystallization temperature (693 K), the critical cleavage strength is so small that the shear-cleavage coefficient α becomes very large, therefore normal fracture always occurs prior to shear deformation. Generally speaking, normal failure and shear failure are two competitive failure modes; when shear deformation becomes difficult, normal failure will act as the failure mode [45].

5. Conclusions

The following conclusions can be drawn in this paper.

- This work confirms that dense and regular shear bands can be created in metallic glasses under multiaxial loading by the small punch test technique at room temperature. The multiplication of radial and circumferential shear bands results from the complex biaxial tensile stress state and the constraint of the geometry. Large shear offset was achieved to accommodate high local plastic strain. Due to the profuse shear bands and large shear offset, macroscopically plastic strain is gained. Even necking phenomenon can occur in metallic glass, and the equivalent plastic strain in the necking is estimated to be over 19.6%.
- Annealing changed the failure modes for the metallic glasses under the small punch test. With increasing temperature, the failure modes changed from circumferential shear fracture to radial shear fracture and finally to radial normal fracture. Both the width of the shear bands and the shear offset decreased with increasing annealing temperature. When the annealing temperature rose above T_x there was no shear deformation, and the failure was a fully radial normal fracture. It is proposed

that the difference in the failure modes was decided mechanically by the shear-cleavage coefficient α, the ratio of critical shear strength to the critical cleavage strength.

- In contrast with the few primary shear bands and catastrophic failure under uniaxial compressive and tensile loading, the propagation of shear bands in metallic glass can be easily controlled by the small punch test technique. This implies that the small punch test is a potential method for studying the evolution of shear bands and, furthermore, can be considered as an effective method to measure the intrinsic ductility of different metallic glasses, and to distinguish their ductile-to-brittle transition behavior more accurately.

References

[1] Johnson WL. MRS Bull 1999;24:42.
[2] Inoue A. Acta Mater 2000;48:279.
[3] Loffler JF. Intermetallics 2003;11:529.
[4] Wang WH, Dong C, Shek CH. Mater Sci Eng R 2004;44:45.
[5] Schuh CA, Hufnagel TC, Ramamurty U. Acta Mater 2007;55:4067.
[6] Wright WJ, Saha R, Nix WD. Mater Trans 2001;42:642.
[7] Zhang ZF, Eckert J, Schultz L. Acta Mater 2003;51:1167.
[8] Pampillo CA, Chen HS. Mater Sci Eng A 1974;13:181.
[9] Sunny GP, Prakash V, Lewandowski JJ. Proceedings of the 2005 international mechanical engineering conference and exposition, IMECE2005-83016. New York: American Society of Mechanical Engineers; 2005.
[10] Zhang ZF, Zhang H, Pan XF, Das J, Eckert J. Philos Mag Lett 2005;85:513.
[11] Bei H, Xie S, George EP. Phys Rev Lett 2006;96:105503.
[12] Sunny G, Lewandowski J, Prakash V. J Mater Res 2007;22:389.
[13] Wu FF, Zhang ZF, Mao SX. J Mater Res 2007;22:501.
[14] Conner RD, Li Y, Nix WD, Johnson WL. Acta Mater 2004;52:2429.
[15] Conner RD, Johnson WL, Paton NE, Nix WD. J Appl Phys 2003;94:904.
[16] Inoue A, Katsuya A, Amiya K, Masumoto T. Mater Trans JIM 1995;36:802.
[17] Katuya A, Inoue A, Amiya K. Int J Rapid Solidif 1996;9:137.
[18] Schuh CA, Nieh TG. Acta Mater 2003;51:87.
[19] Jiang WH, Pinkerton FE, Atzmon M. Acta Mater 2005;53:3469.
[20] Yang B, Nieh TG. Acta Mater 2007;55:295.
[21] Ramamurty U, Jana S, Kawamura Y, Chattopadhyay K. Acta Mater 2005;53:705.
[22] Zhang HW, Jing XN, Subhash G, Kecskes LJ, Dowding RJ. Acta Mater 2005;53:3849.

[23] Lu J, Ravichandran G. J Mater Res 2003;18:2039.
[24] Wu FF, Zhang ZF, Jiang F, Sun J, Shen J, Mao SX. Appl Phys Lett 2007;90:191909.
[25] Mao XY, Shoji T, Takahashi H. J Test Eval 1987;15:30.
[26] Saada AS. Elasticity Theory and Applications. New York: Pergamon Press Inc.; 1974.
[27] Onat ET, Haythornthwaite RM. J Appl Mech 1956;23:49.
[28] Sethi VK, Gibala R, Heuer AH. Scripta Metall Mater 1978;12:207.
[29] Donovan PE, Stobbs WM. Acta Metall 1981;29:1419.
[30] Pekarskaya E, Kim CP, Johnson WL. J Mater Res 2001;16:2513.
[31] Li J, Spaepen F, Hufnagel TC. Philos Mag A 2002;82:2623.
[32] Jiang WH, Atzmon M. Acta Mater 2003;51:4095.
[33] Chen H, He Y, Shiflet GJ, Poon SJ. Nature 1994;367:541.
[34] Wu FF, Zhang ZF, Peker A. Unpublished manuscript.
[35] Nagendra N, Ramamurty U, Goh TT, Li Y. Acta Mater 2000;48: 2603.
[36] Zhang ZF, Wu FF, Gao W, Tan J, Wang ZG, Stoica M, et al. Appl Phys Lett 2006;89:251917.
[37] Jana S, Bhowmick R, Kawamura Y, Chattopadhyay K, Ramamurty U. Intermetallics 2004;12:1097.
[38] Donovan PE. Acta Metall 1989;37:445.
[39] Patnaik MNM, Narasimhan R, Ramamurty U. Acta Mater 2004;52: 3335.
[40] Guo H, Yan PF, Wang YB, Tan J, Zhang ZF, Sui ML, et al. Nat Mater 2007;6:735.
[41] Zhang ZF, He G, Eckert J. Philos Mag 2005;85:897.
[42] Wu FF, Zhang ZF, Peker A, Mao SX, Das J, Eckert J. J Mater Res 2006;21:2331.
[43] Fu XL, Li Y, Schuh CA. Scripta Mater 2007;56:617.
[44] Wu FF, Zhang ZF, Peker A, Mao SX, Eckert J. Phys Rev B 2007;75:134201.
[45] Zhang ZF, Eckert J. Phys Rev Lett 2005;94:094301.
[46] Kanungo BP, Glade SC, Asoka-Kumar P, Flores KM. Intermetallics 2004;12:1073.
[47] Murali P, Ramamurty U. Acta Mater 2005;53:1467.
[48] Raghavan R, Murali P, Ramamurty U. Intermetallics 2006;14:1051.